CFD Prediction of the Effect of Appendages and Leeway on the Force Trend of an Olympic Class Laser Dinghy Hull

Rickard Lindstrand[1], Jeremy Peter[1] and Christian Finnsgård[2,3]

[1]Department of Shipping and Marine Technology, Chalmers University of Technology, Gothenburg, Sweden
[2]SSPA Sweden AB, Research, Gothenburg, Sweden
[3]Centre for Sports Technology, Department of Applied Physics, Chalmers University of Technology, Gothenburg, Sweden

Keywords: CFD, Sailing, Verification & Validation, Tow Tank Testing.

Abstract: The purpose of this paper is to investigate whether the minima in hydrodynamic resistance can be predicted to occur at the same angles of heel and trim in the case of bare hull towing tank tests, bare hull simulations and appendage and leeway simulations. If so, the appendages and the leeway can be rejected from future investigations, which would prove a beneficial advancement, as they impose further complexity to simulations. The results of verification and validation (V&V) included in this paper demonstrate that the numerical method predicted too low resistance. Though the study identifies and systematically investigates possible sources of error, the major source of error was not found. These various possible sources of errors were identified for further research, and as future references for similar cases. Moreover, the simulation results for the variations of heel and trim also require further study. Before a full set of results is available, one cannot make conclusions regarding the angles of heel and trim that lead to minimal resistance. This paper discusses the results and potential avenues of future research, and is a result of an initiative at Chalmers University of Technology focusing on sports and technology.

1 INTRODUCTION

As a result of the hull's complex three-dimensional shape, the flow around the dinghy will differ for different attitudes to the direction of motion. This implies the possibility of locating a minimum of hydrodynamic resistance by sailing at a specific angle of trim and heel. Finding the attitude of minimum resistance can potentially increase performance.

Hydrodynamic resistance is not the only effect that must be considered when altering the angle of heel and trim. The projected area for the centerboard and rudder is decreased when the dinghy is heeled, and this is the case for the sail as well. Moreover, stability could be decreased when trimming on the bow. These effects will not, however, be taken into account in this paper.

Since the weight of the sailor represents more than half of the displacement, the angles of heel and trim are changed by positioning the dinghy's sailor in a certain manner.

At the professional level sailors perform similarly, and thus possibilities like the sailor's position must be exploited in order to gain advantage on the race course. There is little evidence in the literature that an investigation along these lines has been conducted before.

The hull used for this study is the Laser dinghy (see www.laserinternational.org for a description), a four-meter-long dinghy for one sailor. The Laser class has been an Olympic discipline since the 1996 Summer Olympics in Atlanta, and is a strict one-design class, which means that design alterations or additions of any kind are prohibited. Therefore, the manner in which the dinghy is sailed becomes ever more important, and any improvements in sailing practice will consequently improve performance in competitive situations at the international level.

The study resulting with the current paper is a part of an initiative at Chalmers University of Technology. The Olympic motto, "Citius, Altius, Fortius" (Latin for "Faster, Higher, Stronger"), governs everyday life for many engineers, and for the last few years Chalmers has supported a project that focuses on the possibilities and challenges for research combined with engineering knowledge on the area of sports. The initiative has generated

external funding and has gained great acclaim within Chalmers, among staff and students, in the Swedish sports movement, in large companies, as well as within SME's. The project focuses on five sports: swimming, equestrian, floorball, athletics, and sailing.

The paper is composed as follows: Chapter 1 provides the background to the problem and a very brief introduction to the basics of the mechanisms of sailing, the methodology and tow tank test setup. Chapter 2 governs the computational method, while Chapter 3 adresses the numerical method. Chapter 4 and 5 recites the verification and Chapter 6 the validation. Chapter 7 finalises the paer with the concluding remarks.

1.1 Background

The governing equations for the dynamics of a fluid are the Navier-Stokes equation (NS) and the continuity equation. However, it is not possible to fully resolve the flow around a ship, yacht or dinghy with these equations (Larsson and Raven, 2010, section: 9.7.1). This is due to the large separation of scales in the domain and the computational effort required to handle such a separation. While the Laser dinghy is four meters long, the smallest scales in the flow, the Kolmogorov scales, are a mere fraction of a millimetre (Larsson and Raven, 2010). As a result, the resolution of the discretized domain must be incredibly fine in order to fully resolve the flow (Feymark, 2013). The resolving of one of the smallest turbulent scales requires approximately four cells in each spatial direction.

For ship applications, the level of resolution must therefore be limited to that which results in an affordable number of cells. An increase in the cell size leads to a loss of information regarding the smaller turbulent structures. To compensate for this loss of information, turbulence models and near-wall function are introduced to the simulation. Meanwhile, the temporal resolution is neglected all together, as the flow's average quantities are of greater interest than its instant ones (Larsson and Raven, 2010). For example, it may be more valuable to know the average hydrodynamic resistance, rather than the value at each hundredth of a second.

One criterion for neglecting the temporal discretization is that the flow is considered steady, or independent of time. The equations must therefore be adjusted in order to handle averaged quantities. This operation is called Reynolds time averaging, and the new equation is termed the Reynolds time-averaged Navier-Stokes equation (RANS). As the

flow case of the dinghy in flat water is in fact one of steady flow, this paper will employ RANS equations.

1.2 Mechanisms of Sailing

The sail can be understood as a thin wing profile. The wing generates lift and drag, which are defined as the force components that are perpendicular and parallel, respectively, to the apparent wind. The apparent wind is the wind experienced by the sail, i.e., with the boat velocity included (see Figure 1). The point at which the pressure field of the sail can be substituted by one force vector is called the center of effort. As the center of effort is dependent on the pressure distribution, it is not easy to identify, though its location can be estimated at the sail's surface center.
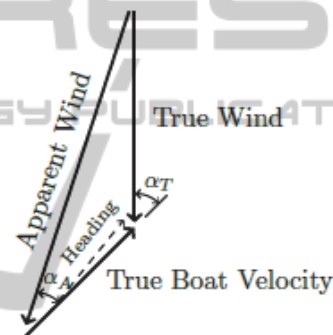

Figure 1: Wind speeds and directions. The leeway is the difference between the heading and the true boat velocity.

The lift of the sail is the only component acting in the yacht's positive direction of motion, and is therefore the only component contributing to propulsion. Furthermore, only one component of the lift is in turn completely aligned with the direction of the yacht. In order for the yacht to move in the right direction, this driving force component must balance the hydrodynamic resistance of the hull, the component of the drag generated by the sail aligned with the opposite direction of the yacht, and the drag generated from the rigging, deck equipment, etc.

The term *leeway* refers to the slight drift of a moving sailing craft toward the leeward side, and is the result of the misalignment of the resultant force of the sail and the direction of motion. This drift is angled in the leeward direction, hence the name leeway. As the center of effort of the sail is not at the same height as the center of pressure for the hull and keel, a heeling moment will also be generated, resulting in the heel angle.

1.3 Methodology

Prior to the investigation of heel and trim variations, a V&V study will be performed. This verification and validation study will be conducted in order to identify the amount of error to be expected from the simulations, and consequently, their relative trustworthiness. Section 4 will further explain the verification procedure.

1.4 Towing Tank Test Setup

Preparation of the dinghy for tow tank testing necessitated modifications. An aluminium frame was fitted to the deck around the cockpit. This frame provided a point at which to attach the towing device and also served to accommodate the weights used to position the dinghy in the desired attitude. The appendages were also removed in order to facilitate what will be called a *bare hull* case. The final modification consisted of the addition of points at which to attach string connected to the measuring devices used to accurately measure heel and trim during speed tests. Figure 2 display the test frame on the deck.

(a) Towing attachment and weight racks on deck.

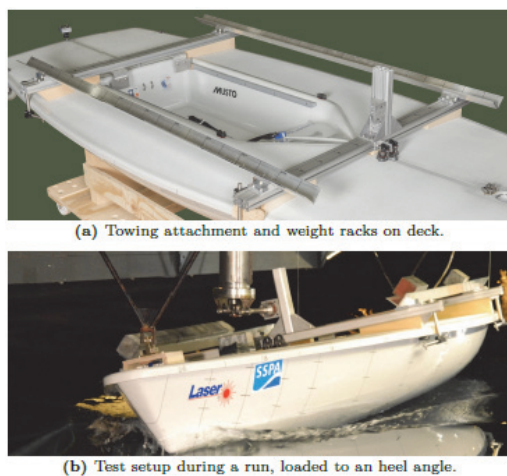(b) Test setup during a run, loaded to an heel angle.

Figure 2: Display of the towing tank test Laser. Photos by SSPA.

The towing device is attached to the top of the vertical aluminium profile. As the towing force is not applied through the center point of the hydrodynamic resistance, a trimming moment is hereby introduced. This moment will not be similar to an actual sailing case, as the towing point does not coincide with the sail's center of effort.

The arm of the towing devise was set up so as to be horizontal for the static cases. This meant that at higher speeds when the dinghy meets with a considerable draft change, the arm would no longer be horizontal, and the towing force would pull the dinghy slightly downward. This would create an increase in displacement, which would in turn affect resistance. Thus, the simulations to be performed could not be set to free sinkage and trim.

Due to limited testing time, the heel tests were only performed as heel to starboard tests.

The brackets that help hold the frame in place are located on the railing of the dinghy, as illustrated in Figure 2b. As the heel angle increased, the starboard side brackets began interfering with the spray from the bow wave. They were therefore removed from that side and from the test rerun, without interference from the frame.

During the test runs, a bailing pump was added on the flooring of the cockpit to guard against excess water. This excess water was a product of the not completely watertight self-bailer device, which was given to leak by the reversal of the test setup back to the starting position in the towing tank after each run.

2 COMPUTATIONAL METHOD

2.1 Governing Equations

The equations that govern fluid flow are derived from basic physical principles and described by the mathematical statements of the conservation laws of physics: the conservation of mass and momentum. The Navier-Stokes equations are derived from the conservation laws and from several underlying assumptions, and are used to predict the resistance forces that result from water pressure and viscous effects.

Basic assumptions. The Navier-Stokes equations are based on the assumptions that the fluid is a continuum, that is, a continuous substance, as opposed to an aggregate of discrete particles.

In the case of water, the flow is commonly considered incompressible, rendering constant the density ρ and the viscosity μ.

The Navier-stokes equation is then time averaged in order to arrive at the RANS equation

Coordinate system. The simulations are not set up to account for changes in sinkage or trim, as a result of the unnatural trimming moment and the vertical force component created by the towing device. The simulation is also assumed to be steady, that is, it is assumed the dinghy will not move relative to waves or in time. In the global Cartesian coordinate system employed here, the origin is at the

bow on the centerline at the undisturbed water level, x is directed sternward, y is directed starboard and z is directed vertically upward.

2.2 Turbulence

2.2.1 Turbulent Flow

Typically, the fluid flow around the hull of a moving ship is turbulent. Turbulent flows are irregular, random and three-dimensional. In such flows, velocity and pressure change continuously, creating within the flow a spectrum of turbulent structures. Despite the irregular nature of a turbulent flow, it is possible to resolve its behaviour with the Navier-Stokes equations (Davidsson, 2003). However, doing so requires that the spatial and temporal discretizations are capable of capturing all scales in the flow. This is not possible for ship applications, as the smallest scales are minuscule in relation to the length of the hull, and this in turn leads to unreasonable computational effort.

To resolve the turbulent flow at issue in the cases here, this study utilizes the Reynolds-averaged Navier-Stokes equation (RANS). This requires that the regular Navier-Stokes equations are averaged over time, a task accomplished by decomposing the instantaneous variables into a mean value $\bar{\varphi}$ and a fluctuating value ϕ' :

$$u_i = \bar{U}_i + u'_i$$
$$P = \bar{P} + p' \tag{1}$$

Insertion of the decomposed terms from (1) into the Navier-Stokes equations gives rise to the Reynolds-averaged Navier-Stokes (RANS) equations. The expression of the incompressible Newtonian fluid in the Einstein notation is:

$$\frac{\partial \bar{U}_i}{\partial t} + \frac{\partial \bar{U}_i \bar{U}_j}{\partial x_j} = -\frac{1}{\rho}\frac{\partial \bar{P}}{\partial x_i} + \frac{\partial}{\partial x_j}\left[\nu\left(\frac{\partial \bar{U}_i}{\partial x_j} + \frac{\partial \bar{U}_j}{\partial x_i}\right) - \overline{u'_i u'_j}\right] \tag{2}$$

This allows for more attention to the mean values, and less to the time histories; indeed, when solving the Navier-Stokes equations, a very fine resolution in time would be necessary in order to resolve the unsteady turbulent flow.

2.2.2 Modelling Turbulence

In the equation (2) the term $\overline{u'_i u'_j}$ appears from the fluctuating values. Known as the Reynolds Stress tensor, this term is an unknown. In order to close the equation system and solve for all the unknowns, the Reynolds stress tensor must be modelled. This is commonly termed the closure problem.

There are various ways to model the Reynolds stress tensor, including the use of algebraic models, one-equation models, two-equation models, algebraic stress models and Reynolds Stress models. Each of these turbulence models varies in terms of computational requirements, accuracy in turbulence modelling and complexity.

Two turbulence models were implemented in the software i: the two-equation Menter's Shear Stress Transport model (SST k-ω) and the explicit algebraic stress model (EASM). A description of these models is available below.

Menter's SST k-ω model. Menter proposed the SST k-ω model in 1992 in order to improve the performance of the near-wall turbulence modelling of the commonly used two-equation k-ε-model (Menter, 1994). The SST k-ω model uses the turbulent kinetic energy k, the turbulence frequency $\omega = \varepsilon/k$ (dimension: s^{-1}) and the Boussinesq assumption to compute the Reynolds stresses. The Boussinesq assumption is the presumed relation linking the Reynolds stress tensor to the velocity gradients and the turbulent viscosity. When a turbulence model uses the Boussinesq assumption, it then qualifies as a "linear eddy viscosity model".

This two-equation turbulence model uses one modelled transport equation for each of the two variables, k and ω. The ω-equation is derived from the ε-equation in the k-ε-model by simply substituting the relation $\varepsilon=k\omega$. Though these equations are not displayed here in detail, it is nevertheless important to understand the manner in which these transport equations are constructed. For both equations, the structure is as follows (Versteeg and Malalasekera, 2007):

$$\text{Rate of change of } k \text{ or } \omega \; + \; \text{Transport of } k \text{ or } \omega \; =$$
$$\text{Transport of } k \text{ or } \omega \text{ by turbulent diffusion}$$
$$+ \text{ Rate of production of } k \text{ or } \omega$$
$$- \text{ Rate of dissipation of } k \text{ or } \omega \tag{3}$$

The SST k-ω model combines the benefits of the Wilcox's k-ω model at the near-wall and the performance at the freestream and shear layers of the k-ε model. This is why Menter's SST k-ω model is suitable for a wide range of CFD applications (Rumsey, 2013). Additionally, assessments of this turbulence model have suggested that it offers superior performance in the case of an adverse pressure gradient boundary layer (Versteeg and Malalasekera, 2007). An adverse pressure gradient leads to lower kinetic energy of the fluid, and hence to a reduction of its velocity. If the pressure increase is large enough, the fluid direction can be reversed; this is what occurs in flow separation, a phenomenon

that typically occurs at the transom of a boat like the Laser. Therefore, this turbulence model seems to be well suited for the current CFD application..

EAS Model. The Explicit Algebraic Stress Model (EASM) proposed in Wallin and Johansson (2000) provides an alternative to linear eddy viscosity models (such as the SST k-ω) based on the Boussinesq hypothesis. Often, linear eddy viscosity models fail to offer satisfactory predictions for complex three-dimensional flows, due to the involvement of the Boussinesq assumption. This leads to nonlinear stress-strain relations in turbulence modelling that contradict the Boussinesq assumption. (Gatski and Speziale, 1993). Nevertheless, owing to their high level of stability, these linear eddy viscosity models are commonly used in the industry (Versteeg and Malalasekera, 2007).

The original algebraic stress model (ASM) model is not often used as a result of robustness issues and frequent instances of singular behaviour (Deng, Queutey, and Visonneau, 2005), both of which the EAS Model addresses by suggesting treatment of the non-linear term by the production-to-dissipation rate ratio, and the number of tensor bases used to represent the explicit solution of those equations. Gatski and Speziale (Gatski and Speziale, 1993) have identified an exact solution for three-dimensional flow involving a ten-term tensor, but require too much computational power. Alternatives discerns that five terms yields acceptable approximation of the solution to the algebraic stress equation (Deng, Queutey, and Visonneau, 2005).

2.3 The Volume of Fluid Method, VOF

The VOF method is a multiphase flow method that computes the interaction of several fluids or phases of a fluid present in the same domain, and obtains the interface between these fluids (Marek, Aniszewski and Boguslawski, 2008). For the purposes of yachting applications, implementation of this method allows for the accurate inclusion of the computation of the free water surface around the hull of the yacht.

The VOF method calls for the solving of, the same Navier-Stokes equation as do single-phase flows. The difference lies in a phase indicating function γ (Hirt and Nichols, 1979). This phase, called the colour function or volume fraction, displays the measure of the mixture of phases in each cell. For instance, if $\gamma = 1$, the cell is completely occupied by phase one, and if $\gamma = 0.3$, 30% of phase one and 70% of phase two are present

in the cell. In terms of yachting applications, the two present fluids are water and air. As air is included in this method, the spatial discretization must extend above the waterline as well. This does, of course, increase the computational effort of the simulation, but it offers a significantly more accurate physical representation of the waves, as will be explained below.

The physical fluid properties used in the Navier-Stokes equation for a multiphase flow is a blend of the properties of the present fluids. In the case of yachting, in which the present fluids are air and water, the computational properties are blended in the following manner:

$$\rho = \rho_w \gamma + \rho_a (1 - \gamma) \qquad \mu = \mu_w \gamma + \mu_a (1 - \gamma) \qquad (4)$$

To track the motion of the interface, a separate transport equation for the colour function is used:

$$0 = \frac{\partial \gamma}{\partial t} + v_i \frac{\partial \gamma}{\partial x_i} \qquad (5)$$

This method does, however, give rise to a numerical problem regarding the smearing of boundaries between the phases over several cells. This smearing denotes that the water surface is constituted by a gradual change in density between water and air. As the water surface is a discontinuity, a jump in density, this smearing represents an unwanted phenomenon. It is a result of the convective averaging being conducted across the water surface. The remedy for this smearing is to implement, in the code, a way to detect the presence of a boundary (Hirt and Nichols, 1998) and treat the bounded areas separately. In the Shipflow software, the smearing problem is addressed by implementation of a compressive discretization scheme, as suggested by Orych, Larsson and Regnstrom (2010).

To render visible the surface of the water, the distribution of the colour function is evaluated. Where $0<\gamma<1$ there is a mixture between the fluids and the free water surface is found. As mentioned, however, the boundary between the phases may be smeared, and therefore a specific value of γ is selected to display the surface.

The VOF method belongs to the class of surface capturing methods. In such methods, the interface between two fluids is computed somewhere inside the domain. The main difference from single-phase surface tracking methods is that, in this case, the dynamics of the air are also computed. In single-phase methods, the water surface geometry forms the top boundary of the domain, and thus these

methods do not take the air into account. The geometry of the top of the domain is then in every time step or iteration updated according to the kinematic and dynamic free surface conditions, and a new grid with new top geometry is generated for the next iteration (Lasson and Raven, 2010). In the VOF method, the free surface conditions are automatically satisfied. Furthermore, surface capturing methods have the advantage of being able to capture overturning waves, drops and complex surface features, if the resolution of the grid is fine enough.

For the purposes of this paper, the advantages of the VOF method in the form of physical representation outweigh the disadvantages of computational cost and numerical instability, and the VOF method will therefore be used for all resistance computations.

3 NUMERICAL METHOD

3.1 Description of the Computational Domain

A structured H-O-grid defines the domain around the hull. This grid layout is desirable because it will generate cells that are roughly aligned with the direction of the flow and fitted to the geometry.

Three different structured grids—the H-O-grid, H-H-grid and O-O-grid—are used to cover each part of the domain. The grid type refers to the shape of the overall domain. The first two grid layouts are displayed in Figures 5a and 5b, respectively. The dome-shaped O-O-grid, used around the appendages, is illustrated by Figure 4b.

The near-wall cells must be quite thin to allow for representation of the velocity profile in the boundary layer, as the gradient of the velocity profile defines the amount of viscous resistance. No wall function was used. The near-wall cells distribution can be observed in Figure 3.
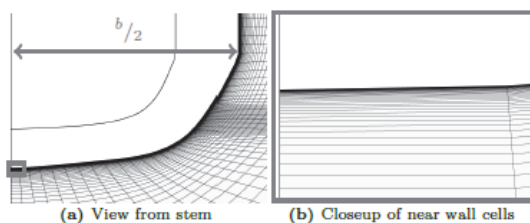

Figure 3: Display of cell density near the walled boundary of the hull.

The H-O-grid layout is used, as displayed in Figure 5a, only in the verification and validation phase, as the hull is then oriented straight against the flow, which means that the case is symmetric. In these cases, the simulations are also symmetric along the centerline.

The H-H-grid, also called box, is used as the main structure for the simulations of the heel and trim variations. Figure 5b demonstrates this grid layout. The geometrical representation of the dinghy's hull and appendages was then added to the domain in the form of overlapping component grids. When these component grids were added, they were also given the selected angles of heel and trim corresponding to the ones obtained at speed during the towing tank tests.
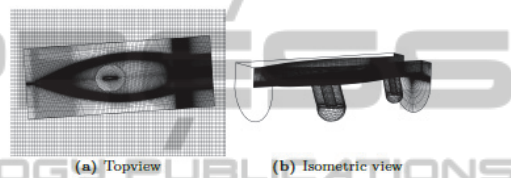

Figure 4: Display of the subgrids used for the investigation cases with appendages and leeway.
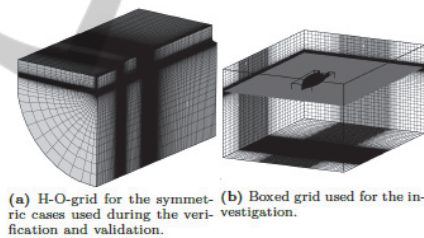

Figure 5: Overview of grid types.

3.2 Boundary Conditions

The boundary conditions for the domain are displayed in the following figure. The slip boundary condition is in practice the same as symmetric, which is why the symmetry boundary is also marked slip. The space above and behind the dinghy is also discretized in two separate grid blocks which are removed from the figure for better visibility.
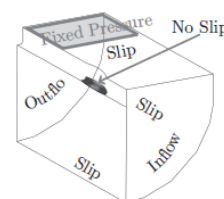

Figure 6: Boundary conditions for the symmetric domain. The same boundary definition is valid for the boxed grid.

4 VERIFICATION METHOD

As the governing equations are implemented in a computer code, the fields of the flow properties must be discretized into smaller fluid particles to which the equations are then applied. The differential equations must be linearized and schemes must be applied in order to estimate the derivatives. The size of the cells in the domain impacts the flow's representation. In general, the smaller the cells, or the larger the amount of cells in the domain, the better the representation of the flow field (Versteeg and Malalasekera, 2007). The number of cells will influence to a great degree just how computationally demanding the simulation will be.

The flow properties are stored in the center of each cell. The cells interact, however, by way of their adjoining boundaries, which means that the quantities must be interpolated to the boundary from the centers. This is done according to an interpolation scheme implemented in the code. To determine how well the interpolation scheme is performing in terms of accuracy, a Taylor expansion of a convective term (a derivative) is conducted (Versteeg and Malalasekera, 2007). When the low order terms are cancelled, the one left with the lowest degree of dependency on the cell size defines the scheme's order of accuracy. The higher order terms in the Taylor series are neglected and the sum is truncated so as to only contain the one defining term.

However, the theoretical order of accuracy, or the decrease in error, might not be observed when refining the grid. This may be attributable to the fact that the refinement of the grid is not completely uniform, to the fact that the wall distance necessary for a turbulence model to be activated is not scaled correctly, or to the fact that the aspect ratio of the cells may change. One further explanation for the inability to obtain the theoretical order of accuracy is that the truncated higher order terms in the Taylor expansion are in fact important for representing the behaviour of the decrease in error.

Any difference between the real flow case and the simulated case in any given quantity is called an error. These errors can be subdivided into two categories: physical modelling errors and numerical modelling errors. Physical modelling errors originate from a faulty model of the physical phenomena at hand, for example, the use of inadequate equations to describe the current phenomena. By contrast, numerical modelling errors derive from the procedures used to solve the equations in the computer. Such errors might include the incorrect rounding off of numbers, incomplete convergence, insufficient spatial discretization, or a diffusive discretization scheme (Larsson and Raven, 2010).

To ensure the trustworthiness of the CFD simulation, the expected error must be quantified (Roy, 2003). Here the quantification of the spatial discretization error will be explained. The other numerical modelling errors are excluded from the verification study; this is possible if the grid refinement factor r is greater than 1.1 (Slater, 2005).

In a validation study, the results of the simulation are compared to the data from tests, rendering indistinguishable the physical errors and the modelling errors.

The verification procedure, called a grid dependence study, aims to observe how a chosen variable, called S, changes according to change in the spatial discretization. In this study, the variable will be the total resistance force of the dinghy. The resistance force will then be plotted as a function of the cell size h for each grid refinement. The data points collected from the simulations of the different grids will then be curve fitted to a certain function and extrapolated to display a hypothetical zero cell size case.

Furthermore, the verification study also offers an accurate view of which errors can be expected as computational effort inevitably increases and the grid becomes more refined. The method for extrapolation consists of an application of the generalized Richardson extrapolation, called least square root method (LSR).

4.1 Richardson Extrapolation

The equation for the Richardson extrapolation is:

$$S_i = S_0 + \alpha h_i^{p_o} \qquad (6)$$

The three unknowns require the use of three different grids. The three solutions form a nonlinear system of equations that have an analytic solution (Roy, 2003) in which r denotes the constant grid refinement factor $r = h_{i+1}/h_i$ and $\varepsilon_{ij} = S_i - S_j$.

$$p_o = \frac{\ln \frac{\varepsilon_{32}}{\varepsilon_{21}}}{\ln r} \qquad (7)$$

$$\alpha = \frac{\varepsilon_{21}}{r^{p_o} - 1} \qquad (8)$$

$$S_0 = S_1 - \frac{\varepsilon_{21}}{r^{p_o} - 1} \qquad (9)$$

4.2 The LSR Method

The drawback of the Richardson interpolation is that it can only be used when the solutions are in the asymptotic range of convergence, which means that

the cell size must be sufficiently small so as to render the higher order terms insignificant (this criterion can be quantified in two ways (Roache, 1998)). This in turn requires that the grids are very fine in order to achieve the asymptotic range (Eca and Hoekstra, 2014). The large computational effort required made the LSR unsuitable for this study (the method for dealing with the scatter of grids considered too coarse for the explained method is proposed in by Eca and Hoekstra, (2014)). The three coefficients to equation 6 are then found by minimizing the following expression:

$$f(S_0, \alpha, p_o) = \sqrt{\sum_{i=1}^{ng} \left(S_i - \left(S_0 + \alpha h_i^{p_o}\right)\right)^2} \qquad (10)$$

Where *ng* is the number of grids used. When using this method, more than three grids are required in order to account for the scatter. This study used seven grids.

4.3 Uncertainty

As the Navier-Stokes equations are not directly solved, numerical models are applied to the simulation. In doing so, not only is the error based on the difference with respect to the test results of interest, but the uncertainty of the simulation itself becomes significant as well (Zou and Larsson, 2010). This uncertainty refers to the interval in which the exact solution is expected to be found.

The purpose of the LSR method is to include the exact solution within the error band with 95% confidence (Eca and Hoekstra, 2006). The appropriate method, an empirical one, is made and adjusted to fit the test results presented at the workshop of Eca and Hoekstra (2006) in a paper of theirs (2014). The computation of uncertainty with the LSR method is governed by the observed order of accuracy p_o, in the following manner:

1. If $p_o > 0$:

$$0.95 \leq p_o \leq 2.05 : U_{sn} = 1.25\delta_{RE} + U_{sd} \qquad (11)$$

$$p_o \leq 0.95 : U_{sn} = min\left(1.25\delta_{RE} + U_{sd},\ 3\delta_{RE}^{12} + U_{sd}^{12}\right) \qquad (12)$$

$$p_o \geq 2.05 : U_{sn} = max\left(1.25\delta_{RE} + U_{sd},\ 3\delta_{RE}^{02} + U_{sd}^{02}\right) \qquad (13)$$

2. If $p_o \leq 0$ and $\sum_{i=2}^{n_g-1} n_i \geq INT\left(n_g/3\right)$, where $n_i = 1$ if $(S_{i+1} - S_i)(S_i - S_{i-1}) < 0$:

$$U_{sn} = 3\delta_{\Delta M} \qquad (14)$$

3. Else :

$$U_{sn} = min\left(3\delta_{\Delta M},\ 3\delta_{RE}^{12} + U_{sd}^{12}\right) \qquad (15)$$

$$\delta_{RE}^{02} = S_i - S_0 = \alpha_{02}h_i^2 \qquad (16)$$

$$\delta_{RE}^{12} = S_i - S_0 = \alpha_{11}h_i + \alpha_{12}h_i^2 \qquad (17)$$

Where:

1. The δ_{RE}^{02} and the δ_{RE}^{12} are obtained from curve fitting the following functions in the same manner as is described in section 4.2.

2. The $\delta_{\Delta M}$:
   Where the ΔM is the maximum data range, $max(|S_i - S_j|)$

$$\delta_{\Delta M} = \frac{\Delta_M}{(h_{n_g}/h_1) - 1} \qquad (18)$$

3. The U_{sd}, U_{sd}^{02} and U_{sd}^{02} are the standard deviations of the curve fitted functions: 6, 16 and 17, the standard deviation is found by minimizing the following expression:

$$U_{sd} = \sqrt{\frac{\sum_{i=1}^{ng} \left[S_i - (S_0 + \alpha_{11}h_i + \alpha_{12}h_i^2)\right]^2}{n_g - 3}} \qquad (19)$$

5 SYSTEMATIC VARIATION OF NUMERICAL PARAMETERS

5.1 Numerical Parameter Study

From the first simulations of this study the resistance was predicted to ~7% below the test data, which was not satisfactory. In order to figure out how to improve the result, the parameters of fluid density ratio, height of domain, turbulence models and local grid refinement were systematically investigated. The outcome of these studies will be presented in this section.

5.1.1 Fluid Density Ratio

This investigation was considered valuable for this study as the default density ratio in the software was set to a nonphysical value. The motivation for using a nonphysical value was that the simulations become more numerically stable for values closer to one, which means two fluids of the same properties. The result of this investigation can be seen in the following figure:
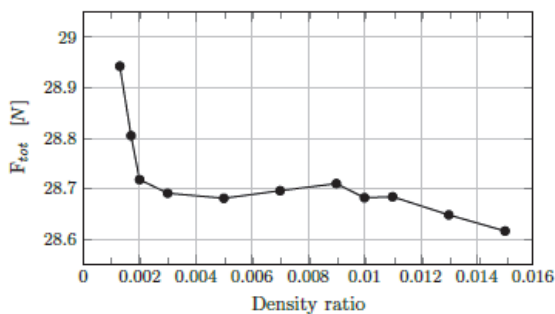
Figure 7: Result of density ratio investigation. The default value in Shipflow was set to 0.01. The percent decrease from 0.0013 to 0.01 is 0.90%.

Notice in Figure 7 that the trend is diverging as the density ratio decreases and goes toward a value of the physical density ratio of 0.0013. No results from values below 0.0013 are reported because these simulations did not converge.

The difference of 0.90% decrease from 0.0013 to 0.01 is not considered insignificant. However, as the results in the region of low density ratio are diverging rapidly, these results are not trustworthy and this quantification shall be viewed with caution.

5.1.2 Domain Height

This investigation was done in order to see the effect of the height of the domain on the resistance but also the free water surface geometry in the transom area. Water on the transom was appearing in the simulations even though the transom evidently was clear during the towing tank tests. The height of the domain here refers to the height of the volume above the water surface, occupied by air.

The number of cells in the z direction was kept constant when the domain height was changed. The results of this investigation can be seen in the following figure:
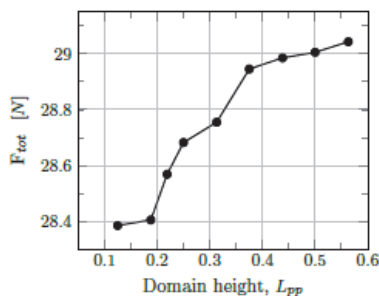

Figure 8: Result of domain height investigation, domain height refers to the height above the static water surface. Default value in Shipflow was set to 0.5.

Notice in figure 8 that the resulting force increases rapidly until 0.375 L_{pp}. The result from the investigation shows a decrease by 2.27% from 0.563 to 0.125, with a plateau starting 0.375 L_{pp}. Domain heights over 0.563 L_{pp} gave diverging simulations.

5.1.3 Turbulence Models

The selected software Shipflow implements two turbulence models: SST k-ω and EASM, see section 2.2.2. As the different turbulence models give good results for different types of flows, both of these were tested in the validation case. The results are presented in table 1.

Table 1: Grid dependency points data.

Density, L_{pp}^{-1}	# cells, M	F_{tot}, [N]	Difference
600	4.7	28.84	-7.14%
3'600	5.9	29.08	-6.50%
7'500	8.9	29.09	-6.46%
30'000	8.9	29.03	-6.65%

Concluded from this investigation is that the SST k-ω model is the superior one for this case. The EASM did not only predict a too-low total resistance, it also took a lot longer to converge. The medium-density grid with the EASM converged with an oscillating trend, and a mean value over 2000 iterations had to be selected. This interval represented roughly two periods of the oscillating behaviour. The SST k-ω was then used for the forthcoming simulations.

5.1.4 Cell Density in the Transom Region

This investigation also originated in having water creeping up on the vertical transom of the dinghy. The cause of this water was thought to be an insufficient resolution of the grid at the corner where the transom meets the bottom of the hull.

A consequence of refining the grid locally in the transom area is the grid density at midships. Stretching functions are used in the meshing tool of the software, which makes the very fine cells gradually grow larger with a certain factor. This makes the cells at midships rather large as a limited number of cells is used to cover the length between perpendiculars. This could have been avoided by adding more cells in this area, but as the transom was the area of interest in this investigation this was not done. The longitudinal direction was selected for refinement. The results of this investigation can be seen in table2.

Table 2: Result of the transom grid refinement investigation. The cell density is in the longitudinal direction, in the region aft of the transom.

# cells, M	Turb. mod.	A_w, [m²]	F_{tot} [N]	Difference
4.9	$k\omega - SST$	3.155	29.00	-6.8%
4.9	EASM	3.168	27.05	-13.0%
5.4	$k\omega - SST$	3.155	29.04	-6.6%
5.4	EASM	3.170	26.64	-14.3%
6.4	$k\omega - SST$	3.154	29.10	-6.44%
6.4	EASM	3.173	26.57	-14.6%

The conclusion of the grid refinement was that the transom water *could be reduced* by refining the transom grid, but it could not be totally cleared. However, the sought gain in resistance was almost negligible and the cost for resolving the flow was significantly increased. This concluded that the transom grid was not the major cause of the too-low predicted total resistance.

5.2 Result of the Verification

After selecting the best settings from the numerical parameter studies, the following verification was obtained (as shown in figure 9 and table 3):
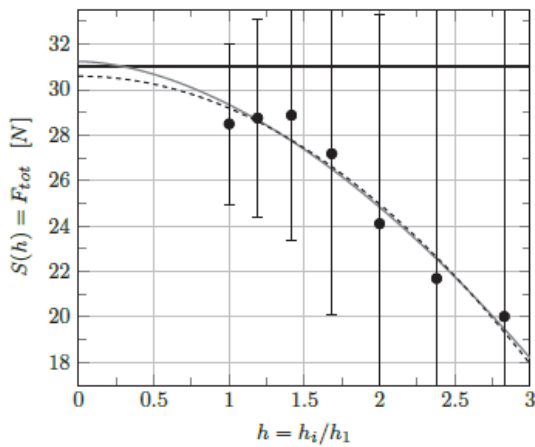

Figure 9: Grid convergence plot. Gray line = curve fit obtained order of accuracy; 1.75. Obtained S0 = 31.24N. Black line = test data; 31.1N.

Evident in this grid-dependence study is that there is a strong grid dependency. This means that a substantial increase in grid definition should be able to eliminate the ~7% error. The problem associated with a further increase is the lack of memory on the machines used to run the simulation during this study. The limit for the available 24GB seemed to be around 14.5 million cells.

Table 3: Grid dependency points data.

Grid	F_{tot} [N]	δ_{RE}/S_{D0}	M cells
0	28.49	8.8%	12.1
1	28.75	8.0%	7.2
2	28.87	7.6%	4.3
3	27.18	13.0%	2.6
4	24.10	22.8%	1.6
5	21.69	30.6%	1.0
6	20.02	35.9%	0.6

A further refinement of r equal to the 4th root of 2 would result in ~20.3 million cells, but a higher refinement factor is probably needed as there is no improvement observed for the finest presented grid.

The conclusion of the grid dependence study is that the grid setup from grid 2 shall be used. To decide which grid refinement results in a reasonable error, the result is weighed against the computation time. As grid 2 gave the best results and did not have the highest computation time, it was selected.

Grid dependency for an appendage and leeway case was not done, as the grid settings for the boxed grid, required to include leeway, were not successfully changed. This was due to lack of knowledge in the meshing tool, which led to an inability to systematically refine the grid.

6 VALIDATION RESULTS AND DISCUSSION

The main investigation of the paper was to see if the minima in resistance could be predicted at the same angles of heel and trim, using the following methods: bare-hull towing tank tests, bare-hull simulations and simulations with appendages and leeway. If this is the case, the more time-consuming asymmetrical simulations needed for handling the leeway can be rejected for future investigations of this kind. The leeway simulations with the appendages are interesting because they represent real sailing conditions in the most accurate way possible in a steady state setup.

The cases that are included in this study are heel variation for zero trim and the trim variation for zero heel. To find a global minima in resistance combinations of heel and trim have to be simulated as well.

A full series of simulations of heel and trim variation was not completed. This was thought to be due to a lack of knowledge in the software, that it is still a young application of the VOF method and that

it is usually handles ships of a very different kind. The results of the simulations that are finished are shown in the following section.

6.1 Heel Variation

The results of the systematic heel variations are presented in figure 10.
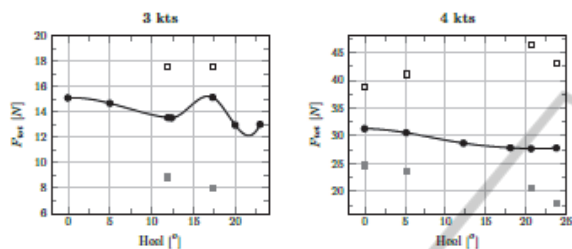

Figure 10: Results of the heel variation. Black = test data, Gray = bare hull simulations, White = Appendages and leeway simulations.

The bare-hull simulations that are finished, and shall be validated against the towing tank test data, are still predicting very low resistance. This is despite the use of the selected numerical parameters from the variation study.

Concluded from the available results from the four-knots-heel variation for the bare-hull cases is that the error is larger than the error obtained in the verification study. The best grid density was then found to be one containing 4.3 million cells and the settings for this grid would now be used for all the simulations during the investigation. The exact grid settings, however, could not be used, as the grid layout will be changed. The grid layout used in the verification study was H-O-grids, explained in section 3.1. For the investigation part, however, the boxed and overlapping grid was used. The reason for this was that the simulations including leeway could not be done in the H-O-grid. The bare-hull simulations were also computed using the boxed grid during the investigation to eliminate the effect of different grid types on a comparison.

The setup of the boxed grid with the selected settings was not done successfully. The reason for this was a lack of knowledge in the meshing tool of the software. A default setting had to be used instead, which prevented the specific settings used in the verification study to be applied.

The default grid settings led to a grid of 7.6 million cells. Recall that this setup is no longer symmetrical through the centreline, and this would therefore have corresponded to 3.8 million in the verification case (where a grid of 4.3 million cells

was preferred). As can be seen in the depiction of the 4 kts case the bare-hull simulations are some ~20% below the test data. Evaluating the results of the verification the following fact can be observed; first, a 20% error would have been predicted for a grid of only 1.6 million cells, and then for a grid of 3.8 million cells an error of 12.1% could have been anticipated. This mismatch between results is a consequence of not being able to use the selected grid settings. This also means that the errors of any simulation with the default grid settings cannot be estimated by the current grid dependence study. The used cell densities are displayed in table 4.

Table 4: Comparison of cell densities at different regions. Densities are expressed in cells per Lpp, y is expressed in the dimensionless length unit.

Region (direction)	Verification (*grid* 2)	Investigation
Upstream (longitudinal)	51	140
Bow (longitudinal)	168	280
Midships (longitudinal)	90	127
Transom (longitudinal)	1010	1600
Wake (longitudinal)	101	476
Overall (radial)	42	160
y_1^+	0.7	1.0

This means that there are no means of evaluating the error in these simulations. As there is no complete series of heel variation, the trends of these series are not available either, all indicating the need for further research.

6.2 Trim Variation

The same goes for the trim variations; there are not enough finished simulations to draw any conclusion.

7 CONCLUDING REMARKS

7.1 Systematic Variation of Numerical Parameters

This section will sum up the study of *systematic variation of numerical parameters*. The study included four different parameters that were expected to have an impact on the predicted resistance of the simulations. These simulations were conducted on grids of 4.5 to 6.5 million cells, which turned out to be somewhere at the ~7% plateau.

Density ratio. The result of this study was that

the most favorable density ratio was 0.01. The resistance, however, could be increased by 0.90% by using the physical density ratio, but as this led to very numerically unstable simulations this was not prioritized.

The conclusion of this investigation was that the results seem to reach a plateau at 0.005 and the fact that a higher density ratio really did make the simulations more stable. Also, as only a small increase in resistance was observed, it was decided to continue the thesis work with the density ratio set to 0.01.

Domain height. The domain height had a significant effect on the resistance but also affected the numerical stability of the simulation. Changing the domain height from 0.563 to 0.125 L_{pp} resulted in a decrease of 2.27%. Above 0.536 the simulations became too numerically unstable. As the domain height was $\sim$0.5 L_{pp} in the previous simulations already, and the threshold of domain height seemed to be 0.536, the positive effect of increased domain height could not be further exploited. The domain height was therefore kept at 0.5 L_{pp}.

Concluded from this investigation was that the domain height shall be set to 0.5 L_{pp}, or in this particular case 2 meters, in order to still be in the region of numerical stability but also to give a resistance as close to the towing tank test result as possible.

Turbulence models. The turbulence models that were implemented for the VOF method in the Shipflow software were EASM and SST k-ω. The previously used SST k-ω was clearly superior to the EASM in this case. As the EASM predicted a twice-as-large error and took substantially more time to converge, the SST k-ω was selected.

Cell density in the transom region. The transom region was refined from the previously used 600 cells per L_{pp}, to 60'000. Only a slight increase in resistance, 0.51%, was noticed. This study could benefit, however, from more thorough investigation, as it was discovered that cell density in other areas of the hull was greatly affected by the transom area. What can be concluded is that an insufficient resolution in the transom area alone is not a major source of error.

Some of the cases run during the main investigation of this study converged to an oscillating behaviour. This can be due to the fact that the flow is not steady state after all. If the flow is unsteady in the transom region, it can result in that the steady state simulation gives this transom water as a result. To test if the flow is unsteady, a transient simulation has to be done, but as the selected

software did not have this option, this was not investigated.

Another way of obtaining an unsteady flow in the simulation is if the waves are not small enough when they are leaving the domain. The remedy for this will then be to increase the overall size of the domain in order for the waves to naturally dampen before reaching the boundaries.

7.2 Investigation

Though no conclusion can be made regarding where the major source of this $\sim$7% error lies, at least some numerical parameters can be ruled out by this study, facilitating further studies in the area.

The study presented in Chapter 5 took most of the time devoted to this project. As no source for the error was found during this study, the thesis work moved on with a modelling setup that was not accurate. As the objective of this paper is to find a minima point of a series of heel and trim variations and not necessarily an absolute value, it was still considered possible. The setting selected during this study was to be used in the investigation to the largest possible extent. All grid density settings were not to be kept completely similar, as the investigation would be performed with the boxed grid setup explained in section 3.1.

As explained in section 5.2, keeping similar grid settings was not possible at all. The even-keel bare-hull case was included in the heel and trim variations but resulted in an even lower resistance than during the verification. As there were larger errors than expected by the grid dependence study, the importance of a good grid became even more evident. However, as the error for the verification case increased so dramatically during the investigation, it can also be concluded that the boxed grid does not perform equally well in this case. This conclusion can be made as the verification case was tested with a non-symmetric H-O-grid as well. The resistance was then 6.9% less than the towing tank test run, compared to the 7.6% of the symmetric case.

To be able to make decisive conclusions, further investigation needs to be conducted. First of all, decide if the VOF method should be used, and then complete the heel and trim variations. The potential flow method implemented in the software was tested after this study, on the verification case, and predicted the resistance within half a percent.

Here follows a list of suggestions for interesting future research:

Simulate the full test matrix. To see get the

global minima in resistance.

Provide sailing recommendations. Evaluate the results of the heel and trim variations and make an instruction of how to achieve highest velocity made good, including a VPP study.

Investigate actual velocities and attitudes. Study the sailors to see which velocities and attitudes are common, to see if there is room for improvement.

Tailor for individual crew weights. To really maximize the effect of the individual sailor, a separate investigation for the weight of the individual sailor could be performed.

ACKNOWLEDGEMENTS

REFERENCES

Davidsson, L., 2003. *An Introduction to Turbulence Models.* Chalmers University of technology, Göteborg.

Deng, Queutey, and Visonneau, 2005. Three dimensional Flow Computation with Reynolds Stress and Algebraic Stress Models. *Engineering Turbulence Modelling and Experiments* (6), pp: 389-398.

Eca and Hoekstra, 2006. *Discretization Uncertainty Estimation Based on a Least SquaresVersion of the Grid Convergence Index.* In: 2nd Workshop on CFD Uncertainty Analysis; Lisabon; October 2006.

Eca and Hoekstra, 2014. A procedure for the estimation of the numerical uncertainty of CFD calculations based on grid renement studies. *Journal of Computational Physics* 262, pp: 104-130.

Feymark, A., 2013. *A Large Eddy Simulation Based Fluid-Structure Interaction Methodology with Application in Hydroelasticity.* PhD thesis. Chalmers, Göteborg.

Gatski and Speziale, 1993. On explicit algebraic stress models for complex turbulent fows. *Journal of Fluid Mechanics* (254), pp. 59-78.

Hirt, C. W. and Nichols, B-D., 1979. *Volume of Fluid (VOF) Method for the Dynamics of Free Boundaries.* Los Alamos Scientific Laboratory, New Mexico.

Hirt and Nichols, 1998. Volume of Fluid (VOF) Method for the Dynamics of Free Boundaries. *Journal of Computaional Physics* (39), pp: 201-225.

Larsson and Raven, 2010. *Ship Resistance and Flow. The Society of Naval Architects and Marine Engineers.*

Marek, Aniszewski and Boguslawski, 2008. *Simplified Volume of Fluid Method (SVOF) for Two-Phase Flows.* Czestochowa University of Technology, Poland.

Menter, F. R., 1994. Two-equation eddy-viscosity turbulence models for engineering applications. *AIAA Journal,* Vol. 32, No. 8, pp: 1598-1605.

Orych, Larsson, and Regnstrom, 2010. *Adaptive overlapping grid techniques and spatial discretization schemes for increasing surface sharpness and numerical accuracy in free surface capturing methods.* 28th Symposium on Naval Hydrodynamics, Pasadena California, pp: 389-398.

Roache, P., 1998. *Verication and Validation in Computational Science and Engineering.* Hermosa Publishers.

Roy, C., 2003. Grid Convergence Error Analysis for Mixed-Order Numerical Schemes. *The American Institute of Aeronautics and Astronautics* (41), pp: 596-604.

Rumsey, C., 2013. *The Menter Shear Stress Transport Turbulence Model.* Web Article. url: http://turbmodels.larc.nasa.gov/sst.html.

Slater, J. W., 2005. *Examining Spatial Grid Convergence.* Web Article. 2005. url: http://grc.nasa.gov/WWW/wind/valid/tutorial/spatconv.html.

Versteeg and Malalasekera, 2007. *An Introduction. to Computational Fluid Dynamics: The Finite Volume Method (2nd Edition).* Prentice Hall.

Wallin, S. and Johansson, A. V., 2000. An Explicit Algebraic Reynolds Stress Model for Incompressible and Compressible Turbulent Flows. *Fluid Mechanics*, Vol. 403, pp: 89-132.

Zou and Larsson, 2010. *A Verication and Validation Study Based on Resistance Submissions.* In: Numerical Ship Hydrodynamics 2010. Workshop, pp: 203-254.